The effect of alkyl spacers on the mixed ionic-electronic conduction properties of n-type polymers

Iuliana P. Maria*, Bryan Paulsen, Achilleas Savva, David Ohayon, Ruiheng Wu, Rawad Hallani, Aniruddha Basu, Weiyuan Du, Thomas D. Anthopoulos, Sahika Inal, Jonathan Rivnay, Iain McCulloch, and Alexander Giovannitti*

I. P. Maria

Department of Chemistry and Centre for Plastic Electronics, Imperial College London London SW7 2AZ, United Kingdom E-mail: iuliana.maria12@imperial.ac.uk

Dr. B. Paulsen, R. Wu, Prof. J. Rivnay Department of Biomedical Engineering, Northwestern University IL 60208, USA

Dr. A. Savva, D. Ohayon, Prof. S. Inal

Organic Bioelectronics Laboratory, Biological and Environmental Science and Engineering Division, King Abdullah University of Science and Technology Thuwal 23955-6900, Saudi Arabia

Dr. R. Hallani, Dr. A. Basu, Dr. W. Du, Prof. T. D. Anthopoulos, Prof. I. McCulloch King Abdullah University of Science and Technology, KAUST Solar Center Thuwal 23955-6900, Saudi Arabia

Prof. J. Rivnay Simpson Querrey Institute, Northwestern University IL 60611, USA

Prof. I. McCulloch

Department of Chemistry, Chemistry Research Laboratory, University of Oxford Oxford, OX1 3TA

Dr. A. Giovannitti

Department of Materials Science and Engineering, Stanford University Stanford, CA 94305, USA E-mail: ag19@stanford.edu

Keywords: n-type polymers, side chain engineering, organic electrochemical transistors, organic bioelectronics, mixed ionic-electronic conduction

Abstract

Conjugated polymers with mixed ionic and electronic transport are essential for developing the complexity and function of electrochemical devices. Current n-type materials have a narrow scope and low performance compared with their p-type counterparts, requiring new molecular design strategies. This work presents two naphthalene diimide-bithiophene (NDI-T2) copolymers functionalized with hybrid alkyl-glycol side chains, where the naphthalene diimide unit is segregated from the ethylene glycol units within the side chain by an alkyl spacer. Introduction of hydrophobic propyl and hexyl spacers is investigated as a strategy to minimize detrimental swelling close to the conjugated backbone and balance the mixed conduction properties of n-type materials in aqueous electrolytes. It is found that both polymers functionalized with alkyl spacers outperform their analogue bearing ethylene glycol-only side chains in organic electrochemical transistors (OECTs). The presence of the alkyl spacers also leads to remarkable stability in OECTs, with no decrease in the ON current after 2 h of operation. Through this versatile side chain modification, our work provides a greater understanding of the structure-property relationships required for n-type OECT materials operating in aqueous media.

1. Introduction

Conjugated polymers that allow simultaneous transport of ionic and electronic charge carriers have experienced a surge of interest for a wide range of applications, [1] including energy neuromorphic storage, [2-4] computing, [5,6] electrochromic devices^[7] bioelectronics.^[8-11] A particular device which has benefitted from their mixed conduction properties is the organic electrochemical transistor (OECT). Due to their soft nature and compatibility with living systems, conjugated polymers have emerged as ideal channel materials for OECTs employed to transduce signals at the interface with biological media.^[12] For many applications, OECTs operate as amplifying transducers, converting small changes in the gate voltage into large changes in the channel current, with an efficiency given by the transconductance, $g_{\rm m}$. [13] The transconductance shows a direct dependence on the volumetric capacitance (C^*) and the charge carrier mobility (μ) of the active material, as well as the channel thickness (d), length (L) and width (W), the gate voltage (V_G) and the threshold voltage (V_T). In the saturation regime, the transconductance is given by $g_m = \frac{W d}{L} \mu C^* (V_T - V_G)$. With both ionic and electronic elements captured, the μC^* term is the key parameter for evaluating the mixed conduction properties of the active material and establishing structure-property relationships for high performing OECTs.[14]

A successful approach to promote OECT operation in aqueous media is to exchange the hydrophobic alkyl side chains of solution-processable conjugated polymers with hydrophilic ethylene glycol (EG) units. Several studies have demonstrated that EG side chains endow conjugated polymers with the ability to swell in aqueous electrolytes and facilitate the transport of hydrated ions.^[15–21] Through careful engineering of the side chain length and density, p-type polymers can now operate in aqueous-based OECTs with μC^* products higher than 100 F cm⁻¹ V⁻¹ s⁻¹.^[15,16,22] The first example of a n-type OECT operating in aqueous electrolytes^[18] was

accomplished by functionalization with a polar EG-based side chain of a widely studied n-type backbone motif, the naphthalene tetracarboxylic diimide-bithiophene (NDI-T2),^[23] forging new directions for OECT-based technologies. One research area that has greatly benefited from electron-transporting OECT materials is enzymatic sensing of metabolites such as lactate or glucose.^[24,25] Additionally, access to n-type polymers enabled the development of complementary circuits based on electrochemical operation in aqueous media, with prospects for signal amplification with low power consumption.^[26]

However, despite recent progress, n-type OECT materials still suffer from low electron mobilities and show μC^* products approximately three orders of magnitude lower than their p-type counterparts. As applications for n-type polymers continue to mature, there is a growing need for strategies that can optimize both their ionic and electronic transport properties and hence improve the g_m of the device. The lower electronic charge carrier mobilities of n-type OECT materials can be attributed to several reasons. For instance, localization of the electronic charges on the acceptor units of the polymer backbone^[27] may lead to strong electrostatic interactions with the counterions, in contrast with p-type analogues where charges are often delocalized over several repeat units. Additionally, several investigations of both p- and n-type materials have shown that electrochemical doping can lead to drastic morphological changes as the polymer film reorganizes to accommodate ions and water molecules from the electrolyte.^[28–32] Excessive hydration of the film can lead to disproportionate swelling of the amorphous and ordered domains, disrupting the interconnections between crystallites and negatively impacting the transport of electronic charges.^[31,32]

To improve the performance of OECTs, several strategies have been explored to limit the swelling of the channel material and to balance the ionic and electronic transport properties. These include optimization of the processing conditions of the channel material, [31] variations in the concentration and nature of the aqueous electrolyte [28,29,32] and chemical design

strategies.^[19,20] In a previous study, we showed that the swelling of a n-type channel material could be tuned by synthesizing random polymers bearing both hydrophilic EG and hydrophobic alkyl side chains in different ratios.^[19] EG percentages higher than 50% were required for OECT operation in aqueous electrolytes, while polymers with lower EG percentages could only perform moderately well in organic field-effect transistors (OFETs). It is noteworthy that increasing the EG side chain density impaired the electron mobility of the conjugated polymer, although a higher capacitance could be obtained. A good balance between these two factors was achieved for the polymer with a EG percentage of 90%, which showed the highest μ C* and normalized g_m within the series.^[19] While this approach elucidated key design principles, the use of random copolymers as benchmark materials for OECT-based technologies is not ideal due to potential batch-to-batch variations.^[33]

In the study presented herein, the alternating NDI-T2 backbone motif is functionalized with hybrid alkyl-glycol side chains. The length of the alkyl unit is varied to control the swelling of the polymer and improve the electronic charge transport properties while maintaining sufficient ionic charge transport. A similar side chain engineering approach was recently employed for the design of p-type copolymers, [17,34] however is yet to be investigated for n-type OECT materials. The relative position of the alkyl unit with respect to the conjugated backbone has been shown to have significant impact on the electronic transport properties. Specifically, the polymers with the hydrophobic alkyl unit adjacent to the backbone showed improved long-range ordering and electron mobility in organic field-effect transistors (OFETs). [35] For polymers designed for aqueous-based OECTs, this may also prevent encroachment of ions at the location of polaron delocalization along the backbone, avoiding charge trapping and thus potentially increasing the charge carrier mobility.

Motivated to explore this design strategy in electrochemical devices, a series of NDI-T2 copolymers functionalized with hybrid alkyl-glycol chains, attached via an alkyl spacer, were

investigated. Starting from the previously reported n-type polymer p(gNDI-gT2),^[18] two derivatives featuring either a propyl (C₃) or a hexyl (C₆) spacer were prepared (**Figure 1a**) and their electrochemical properties were studied in aqueous electrolytes. Our findings show that the introduction of alkyl spacers can be used to limit detrimental swelling in the aqueous environment, improve the performance and long-term stability of the n-type polymer during operation in OECTs.

2. Results and Discussion

The synthetic route to p(C3-gNDI-gT2) and p(C6-gNDI-gT2) is shown in Figure 1a. Monomers C3-gNDI and C6-gNDI were prepared from 2,6-dibromonaphthalene-1,4,5,8tetracarboxylic dianhydride using a one-pot procedure as previously reported, [18] which allowed both functionalization with the alkyl spacer at the imide position and extension with the EG unit via an ester linkage in one step. 2,6-Dibromonaphthalene-1,4,5,8-tetracarboxylic dianhydride was treated in turn with 3-amino-1-propanol and 6-amino-1-propanol, followed by an excess of 2-[2-(2-methoxyethoxy)ethoxy]acetic acid to afford monomers C3-gNDI and C6-gNDI, respectively as detailed in the Supporting Information. Purification of C3-gNDI (36% yield) and C6-gNDI (46% yield) was achieved by preparative gel permeation chromatography, whereas column chromatography resulted in lower yields (<15%), most likely due to cleavage of the ester group when using methanol-containing solvent mixtures as the eluent. This observation is in agreement with recent findings describing the synthesis of other NDI-T2 copolymers with polar side chains containing an ester linkage. [36] Copolymerization via Stille coupling was carried out following an optimized protocol, which has been previously shown to increase the yield of the chloroform soluble fractions for p(gNDIgT2).[37] Accordingly, C3-gNDI and C6-gNDI were reacted with equimolar quantities of the stannylated comonomer gT2 in DMF at 80 °C to give p(C3-gNDI-gT2) and p(C6-gNDI-gT2)

in a yield of 83 and 70%, respectively. The polymer bearing EG-only side chains, p(gNDI-gT2), used for comparison in this study was synthesized as previously reported.^[37] The presence of the ester linkage within the polymer side chain following purification was confirmed by IR spectroscopy (**Figure S5**). All polymers showed good solubility in chloroform at room temperature and moderate solubility in chlorobenzene at 80 °C.

Gel permeation chromatography was employed to estimate the molecular weights of the polymer series, using polystyrene standards and chloroform as the eluent at 40 °C. The number-average molecular weights (M_n) were found to be in the 16.8 to 32.4 kDa range with dispersities (D) between 2.27 and 3.04, as summarised in **Table 1**. It should be noted that all polymers showed bimodal molecular weight distributions, most likely due to aggregation in solution (**Figure S6**) which may lead to overestimation of the molecular weights. To further investigate the molecular weight distributions, matrix-assisted laser desorption/ionization time-of-flight spectrometry (MALDI-ToF) measurements were carried out, showing polymer chains up to 7–9 repeat units (**Figure S7**). Due to discrimination of high molecular weight species in polydisperse polymers by MALDI-ToF,^[38] the number-average molecular weight of the polymers is expected to be an intermediate value between the two techniques. Similar findings have been previously reported when attempting to determine the molecular weight distribution of polymers with polar side chains by GPC or MALDI-ToF measurements.^[19,36,39] All polymers show good thermal stability with 5% weight-loss temperatures above 300 °C, as determined by thermogravimetric analysis under inert atmosphere (**Table 1**, **Figure S8**).

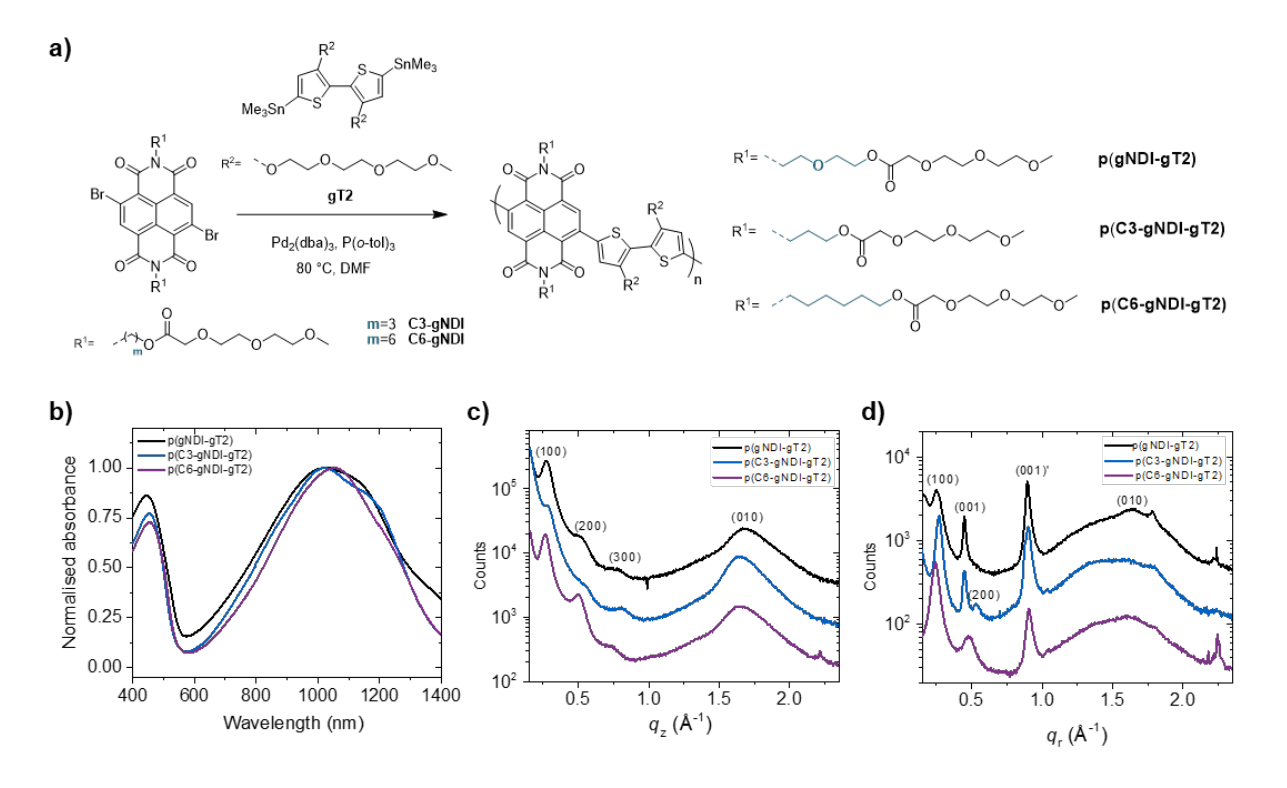


Figure 1. (a) Synthesis and chemical structures of the polymers. (b) Normalized UV-Vis-NIR absorption spectra of the polymer thin films on glass substrates (measurements of the polymers in solution are presented in the Supporting Information). GIWAXS of neat as-cast films showing (c) the out-of-plane (q_z) and (d) the in-plane (q_r) line cuts of each polymer.

The optoelectronic properties of the polymer series are summarized in **Table 1**. Photoelectron spectroscopy in air (PESA) measurements were employed to determine ionization potentials (IP), which were found to be comparable (~5.1 eV) across the series. Similarly, the electron affinities (EA) were found to be ~4.0 eV for all polymers, as determined by cyclic voltammetry of the thin films in 0.1 M tetrabutylammonium hexafluorophosphate (TBAPF₆) in acetonitrile (**Table 1**, **Figure S9**). As expected, due to the electronic decoupling of the NDI core and the substituents at the imide position, modulation of the side chain structure gave negligible differences in the EA.^[40]

Table 1. Properties of the copolymers

Polymer	$M_n[D]$ [kDa] ^{a)}	Repeat units ^{b)}	$E_{\rm g}$ [eV] ^{c)}	EA [eV] ^{d)}	IP [eV] ^{e)}
p(gNDI-gT2)	16.8 [3.04]	7	0.8	4.0	5.1
p(C3-gNDI-gT2)	32.4 [2.27]	9	0.9	4.1	5.2
p(C6-gNDI-gT2)	20.2 [2.68]	8	0.9	4.0	5.1

a) Number-average molecular weight (M_n) and dispersity (D) (GPC versus polystyrene standards in chloroform);

The UV-Vis absorption spectra of the polymers as thin films and in solution are shown in **Figure 1b** and **Figure S10**, respectively. All polymers show a dual-band absorption profile characteristic of donor-acceptor polymers, [41,42] with a high energy band ascribed to the π - π * transition ($\lambda_{max} \sim 450$ nm) and a low energy band ascribed to intramolecular charge transfer (ICT, $\lambda_{max} \sim 1050$ nm). The optical band gaps were estimated from the absorption onset of the thin film spectra, resulting in similar values of 0.8–0.9 eV across the series (**Table 1**). Interestingly, the p(C3-gNDI-gT2) thin film shows aggregation features with a low energy shoulder peak at 1172 nm, suggesting enhanced interchain interactions. [43]

To investigate the changes of the polymer microstructure upon introduction of hybrid alkylglycol side chains, grazing incidence wide angle X-ray scattering (GIWAXS) measurements
were carried out. The line-cuts of the as-spun thin films are presented in **Figure 1c** and **d**, while
the 2D GIWAXS patterns and relevant peak parameters are included in the Supporting
Information (**Figure S18**, **Table S1–S3**). The general microstructure is similar to previously
reported NDI-T2 analogues, [19,44,45] showing a mixture of edge-on and face-on crystallites with
varying degrees of isotropic character. The enhanced out-of-plane π -stack scattering and inplane backbone scattering indicates a predominantly face-on orientation across the series.

^{b)} Determined by MALDI-ToF; ^{c)} Optical band gap estimated from the thin film absorption onsets; ^{d)} Determined by cyclic voltammetry of the polymer thin films on ITO coated glass substrates in acetonitrile with 0.1 M tetrabutylammonium hexafluorophosphate as the supporting electrolyte; ^{e)} Measured by photoelectron spectroscopy in air.

Notably, the polymer having a short C_3 -alkyl spacer, p(C3-gNDI-gT2), shows stronger out-of-plane π -stack scattering compared to p(gNDI-gT2) and p(C6-gNDI-gT2).

All films show evidence of three orders of out-of-plane lamellar scattering. As expected, p(C3gNDI-gT2) with the shortest overall length of the side chain shows a contracted lamellar dspacing, both in- and out-of-plane, compared with the rest of the series. Increasing the fraction of alkyl units led to an increase in in-plane lamellar scattering and the emergence of a second order lamellar peak. Conversely, introduction of alkyl spacers led to a decrease in the magnitude of in-plane backbone scattering peaks. In particular, the (001) scattering magnitude is indistinguishable for p(C6-gNDI-gT2), while the (001)' peak persists. Previous studies have shown that NDI-T2 based polymers display two polymorphs that represent two cases of cofacial registration: Form I (noted as (001)) where the chains align with a segregated alternating NDI-to-NDI and T2-to-T2 cofacial registration producing a longer backbone periodicity, and Form II (noted as (001)') where the chains align with a mixed NDI-to-T2 cofacial registration producing a shorter backbone periodicity. [46] Here, it appears that introduction of a C6-alkyl spacer within the side chain produced a preference for Form II and disrupted Form I. Interestingly, the presence of only Form II stacking did not result in a transition to predominately edge-on orientation, as it was previously reported for analogous alkyl-substituted polymers.^[47]

To quantitatively assess the molecular packing order, Fourier transforms of the in-plane pseudo-Voigt peak fits were fit to extract estimates of the non-cumulative disorder due to lattice parameter fluctuations (e_{rms}), the cumulative paracrystalline disorder (g) and the disorder associated coherence length (ξ) in both backbone and lamellar directions (**Table S1-S3**).^[48] Across all series, cumulative paracrystalline disorder dominated. Notably, p(C3-gNDI-gT2) crystallites showed the largest lamellar and backbone ξ values of 213 and 345 Å, calculated from the (100) and (001') peaks, respectively.

The electronic charge transport properties of the polymers were first assessed in their dry state by fabricating OFET devices with a bottom-gate (Si) bottom-contact (Ti/Au) architecture (**Figure S11**) and extracting the electron mobility in the linear regime. As previously reported for other NDI-T2 copolymers functionalized with EG side chains, [18,19] the OFET mobilities were found to be up to 4 orders of magnitude lower than that of their alkylated analogue, p(NDI2OD-T2). [23] Both polymers bearing alkyl spacers show an improvement in the OFET mobility compared with the EG-only analogue. The derivative functionalized with a short C3-alkyl spacer, p(C3-gNDI-gT2), was found to have the highest electron mobility of 9.2×10^{-4} cm² V⁻¹ s⁻¹ relative to p(gNDI-gT2) (2.2×10^{-4} cm² V⁻¹ s⁻¹) and p(C6-gNDI-gT2) (6.3×10^{-4} cm² V⁻¹ s⁻¹). This is likely attributed to its longer coherence length in both the backbone and lamellar directions and larger π -stack scattering intensity relative to the rest of the series. The enhanced coherence length along the backbone direction is expected to be particularly important as NDI-T2 copolymers have previously shown anisotropic charge transport that favors the backbone direction over the lamellar direction, [47] though the OFET mobilities of p(gNDI-gT2) and p(C6-gNDI-gT2) do not correlate with ξ along the backbone direction.

Several studies have demonstrated a correlation between the mixed ionic-electronic transport properties of OECT channel materials and their extent of swelling when exposed to aqueous electrolytes.^[19,20,32] The effect of functionalization with alkyl spacers on the swelling ability of the polymers was investigated using quartz crystal microbalance with dissipation monitoring (QCM-D). In agreement with previous findings,^[19,20] the largest degree of passive swelling was observed for the polymer with the largest fraction of hydrophilic side chains (p(gNDI-gT2), 44%), followed by the polymer bearing a short C₃-alkyl spacer (p(C3-gNDI-gT2), 28%) and an extended C₆-alkyl spacer (p(C6-gNDI-gT2), 13%) (**Figure S12**).

The influence of the alkyl spacers on the electrochemical activity of the polymers in aqueous electrolytes was further investigated by cyclic voltammetry (CV) and spectroelectrochemistry

measurements. As shown in Figure 2a, all polymers can be oxidized and reduced within the electrochemical stability window of the electrolyte. Polymers p(gNDI-gT2) and p(C3-gNDIgT2) show comparable reduction onsets of approximately –0.1 V vs. Ag/AgCl. Upon extending the spacer to a C₆-alkyl unit, the reduction onset shifts by $\Delta V = 0.1 \text{ V}$ to more negative values. As the polymers have similar EAs, this shift is most likely a result of the lower degree of swelling and potentially a lower ionic mobility for p(C6-gNDI-gT2).[19,20] Although oxidative processes can be also observed (Figure 2a), the current response is lower compared to that measured for reduction. The electrochemical activity of the polymers in aqueous electrolytes was further evaluated by monitoring the evolution of the UV-Vis spectra during the reduction of the polymers between 0 V to -0.8 V vs. Ag/AgCl. All polymers showed a gradual reduction in the intensity of the ICT band and a simultaneous increase in the intensity of new absorption features between 810-830 nm and 500-650 nm (Figure 2b, Figure S14). These spectral changes are consistent with the formation of a polaronic species upon electrochemical reduction, as described previously.^[2] In agreement with the findings from the CV measurements, p(C6-gNDI-gT2) requires a higher bias to achieve similar degrees of charging and polaron formation with respect to the other polymers (Figure 2c).

During the electrochemical reduction of the polymer thin film, cations migrate into the polymer film to compensate for the electronic charges on the polymer backbone. [2] As in aqueous media the dopant ions are surrounded by a hydration shell, the polymer is also expected to uptake several molecules of water during the charging process. [28,29,32] The changes in the mass of the polymer films during charging (active swelling) were investigated using electrochemical QCM-D measurements in aqueous electrolytes. As expected, all polymers show mass uptake during the reduction of the polymer and mass loss during the oxidation of the reduced polymer (**Figure 2d**). Interestingly, partial retention of the accumulated mass is observed for all polymers after completing the charging/discharging cycle, indicative of strong binding of water

molecules to the polymer backbone or side chains. The magnitude of the swelling triggered by charging follows the same trend as the passive swelling, decreasing in the order p(gNDI-gT2) > p(C3-gNDI-gT2) > p(C6-gNDI-gT2)). For instance, at a bias of -0.3 V vs. Ag/AgCl, the mass accumulated within the p(C6-gNDI-gT2) film is half of the mass accumulated within p(gNDI-gT2). A similar trend is observed upon monitoring the mass uptake for two additional doping cycles (**Figure S13**). In agreement with previous studies, [19,20] decreasing the density of hydrophilic EG units, in this case correlated with introduction of alkyl spacers within the side chain, leads to a lower swelling ability in aqueous electrolytes. In addition, due to a higher onset for reduction, p(C6-gNDI-gT2) most likely achieves a lower degree of charging at -0.3 V vs. Ag/AgCl and shows a lower number of injected hydrated cations relative to p(gNDI-gT2) and p(C3-gNDI-gT2).

The findings from the swelling analysis with and without applying a bias show that the inclusion of alkyl spacers is a successful strategy for modulating the degree of swelling of polymer films. Previous work has shown that employing redox-active polymers with low swelling abilities can hinder ion penetration into the bulk of the material, leading to undesirable high reduction potentials.^[19] Notably, the hybrid side chains with C₃- or C₆-alkyl spacers provide an appropriate balance between hydrophilic and hydrophobic units for controlling the swelling of the polymer, whilst also achieving electrochemical reduction at low potentials.

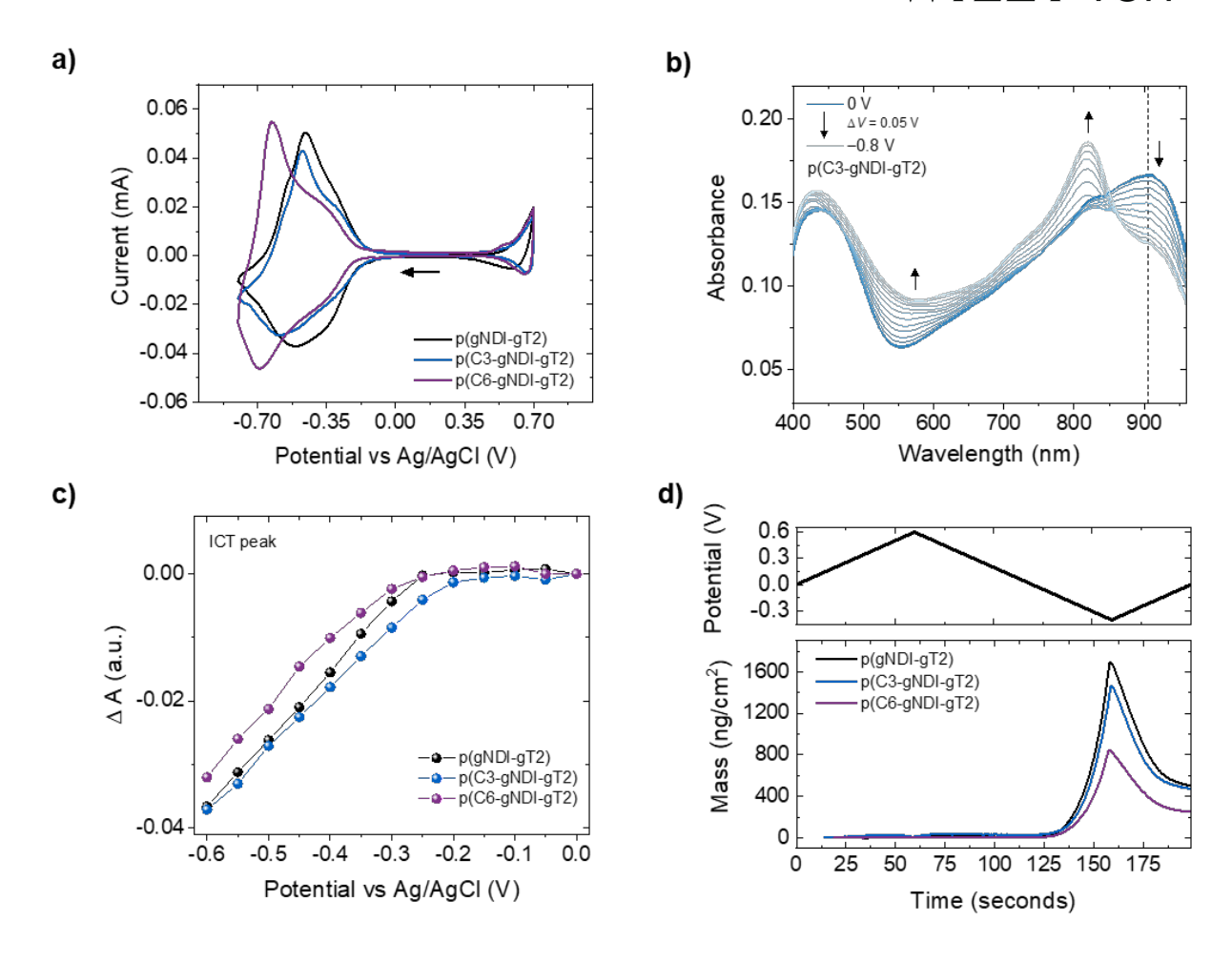


Figure 2. (a) Cyclic voltammetry of the polymer films on ITO coated glass substrates with a scan rate of 100 mV s⁻¹ and a Ag/AgCl reference in a 0.1 M NaCl aqueous solution with a low O₂ concentration, showing the 2nd scan. Arrow indicates the direction of the scan. (b) Evolution of the UV-Vis absorption spectrum of p(C3-gNDI-gT2) during charging between 0 and -0.8 V vs. Ag/AgCl with a scan rate of 50 mV s⁻¹ in a 0.1 M NaCl aqueous solution at low O₂ concentration. The spectroelectrochemical measurements for p(gNDI-gT2) and p(C6-gNDI-gT2) are included in the Supporting Information (**Figure S14**). (c) Relative changes of the absorption spectrum showing the difference between the absorbance of the ICT peak recorded with bias and the neutral polymers for charging between 0 V to -0.6 V vs. Ag/AgCl in steps of 50 mV. (d) EQCM-D for the polymer films for one doping cycle (between 0.6 and -0.40 V vs.

Ag/AgCl) in a 0.1 M NaCl aqueous solution. The second and third charging/discharging cycles are included in the Supporting Information (**Figure S13**).

After identifying the impact of side chain substitution on the redox-potentials and swelling behavior, we analyzed the performance of the polymers in OECTs. **Figure 3a** shows the transfer curves of the OECTs in a 0.1 M NaCl aqueous solution in ambient conditions (see **Figure S15** for output curves) and **Table 2** summarises the OECT parameters. Notably, both polymers functionalized with alkyl spacers show a higher thickness-normalized peak transconductance compared with p(gNDI-gT2), as shown in **Figure 3b**. The derived products of the material-dependent parameters (μ C*) follow the same trend, increasing from 0.06 to 0.13 and 0.16 F cm⁻¹ V⁻¹ s⁻¹ when going from p(gNDI-gT2) without a spacer to p(C3-gNDI-gT2) and p(C6-gNDI-gT2). While p(C3-gNDI-gT2) and p(C6-gNDI-gT2) show a comparable peak g_m and μ C*, increasing the length of the alkyl spacer shifts the potential required to achieve these to higher values. The threshold voltages (V_T) follow the same trend as the reduction onsets determined by CV, with a higher V_T of 0.37 V for p(C6-gNDI-gT2) bearing an extended spacer relative to both p(C3-gNDI-gT2) and p(gNDI-gT2) (0.25 and 0.26 V, respectively).

Table 2. OECT performance of polymers

Polymer	g_{m} [S cm ⁻¹] ^{a)}	<i>V</i> _T [V] ^{b)}	$[\mu C^*]$ [F cm ⁻¹ V ⁻¹ s ⁻¹] ^{c)}	C* [F cm ⁻³] ^{d)}	$\mu_{e \text{ (OFET)}}$ [cm ² V ⁻¹ s ⁻¹] ^{e)}
p(gNDI-gT2)	0.13	0.26	0.06	221	2.2 ×10 ⁻⁴
p(C3-gNDI-gT2)	0.34	0.25	0.13	72	9.2×10^{-4}
p(C6-gNDI-gT2)	0.37	0.37	0.16	59	6.3×10^{-4}

^{a)} OECT peak transconductance measured at $V_G = 0.5$ V for p(gNDI-gT2) and p(C3-gNDI-T2) and $V_G = 0.6$ V for p(C6-gNDI-gT2) normalized by thickness; ^{b)} Threshold voltage extracted from the $\sqrt{I_D}$ versus V_G plot; ^{c)} [μC^*] estimated from the transfer characteristics of the OECT with known channel dimensions and biasing conditions; ^{d)} Determined from the electrochemical impedance spectra of the polymers coated on Au electrodes (500 × 500 μ m) in a 0.1 M NaCl aqueous solution (V = -0.6 V vs. Ag/AgCl); ^{e)} OFET electron mobility extracted from bottom-gate bottom-contact transistors in the linear regime.

The trends in the μC^* products across the series were further investigated by performing electrochemical impedance spectroscopy (EIS) to determine the volumetric capacitance (C^*) at an offset potential of – 0.6 V vs. Ag/AgCl in a 0.1 M NaCl aqueous solution (**Figure S16**). The polymer with the highest density of EG units, p(gNDI-gT2), shows the largest C^* of 221 F cm⁻³. The C^* decreases upon functionalization with alkyl spacers, with values of 72 F cm⁻³ for p(C3-gNDI-gT2) and 59 F cm⁻³ for p(C6-gNDI-gT2) (**Table 2**). Interestingly, the C^* decreases by a factor of three when going from p(gNDI-gT2) to p(C3-gNDI-gT2) and greater than three for p(C6-gNDI-gT2), which is most likely correlated with the decrease in the fraction of hydrophilic side chains and swelling ability. However, due to its higher reduction potentials (**Figure 2a**), p(C6-gNDI-gT2) requires a higher bias to achieve a comparable degree of charging, which is expected to contribute further to lowering its C^* . It should be noted that although bandwidth measurements were employed to extract the OECT electron mobility independently, ^[49] no accurate values could be determined due to the low currents typically observed for thin n-type OECTs. However, as both p(C3-gNDI-gT2) and p(C6-gNDI-gT2)

show a lower C^* relative to p(gNDI-gT2), the higher μC^* product is indicative of an increase in the OECT electron mobility upon introduction of alkyl spacers.

In addition to the performance of the device, an important requirement for OECT-based applications is long-term stability during operation. Stability measurements were carried out for all polymers by monitoring the drain current upon applying gate voltage steps over 150 min. The current response of p(gNDI-gT2) and p(C3-gNDI-gT2) was first recorded at $\Delta V_{\rm G}$ = 0.5 V, which represents the gate voltage at which their peak $g_{\rm m}$ was measured (**Figure S17**). The ON current of p(gNDI-gT2) decreases by \sim 7% after the first 60 min of operation, after which it recovers partially towards the end of the measurement. Polymer p(C3-gNDI-gT2) shows a steady increase in the ON current, with a total increase of ~19% over 150 min. When the gate voltage is increased to $\Delta V_{\rm G} = 0.6 \text{ V}$, p(gNDI-gT2) shows much lower operational stability, retaining only 67% of the ON current after 150 min (Figure 3c). The current response of p(C3-gNDI-gT2) at $\Delta V_{\rm G} = 0.6$ V is similar to the recordings at $\Delta V_{\rm G} = 0.5$ V with a total increase of ~19%, indicative of improved stability at higher biases upon functionalization with the C₃-alkyl spacer. Although no deterioration in the current is observed, the steady change in the ON current shown by p(C3-gNDI-gT2) at both $\Delta V_{\rm G} = 0.5$ V and $\Delta V_{\rm G} = 0.6$ V could hinder its use for long-term sensing applications, where these fluctuations in current could interfere with the response of the device to biological events or detection of analytes. Remarkably, p(C6gNDI-gT2) shows very stable operation, with no change in the original current for over 2 h of on-off switching at $\Delta V_{\rm G} = 0.6$ V, corresponding to the bias at which the peak $g_{\rm m}$ is observed (**Figure 3c**). The more stable current response of p(C3-gNDI-gT2) and p(C6-gNDI-gT2) compared with p(gNDI-gT2) is most likely attributed to their lower extent of swelling during charging, as determined by EQCM-D. These results demonstrate that optimization of the length of the alkyl spacer within the side chains is a successful strategy for improving the long-term operational stability of OECT materials.

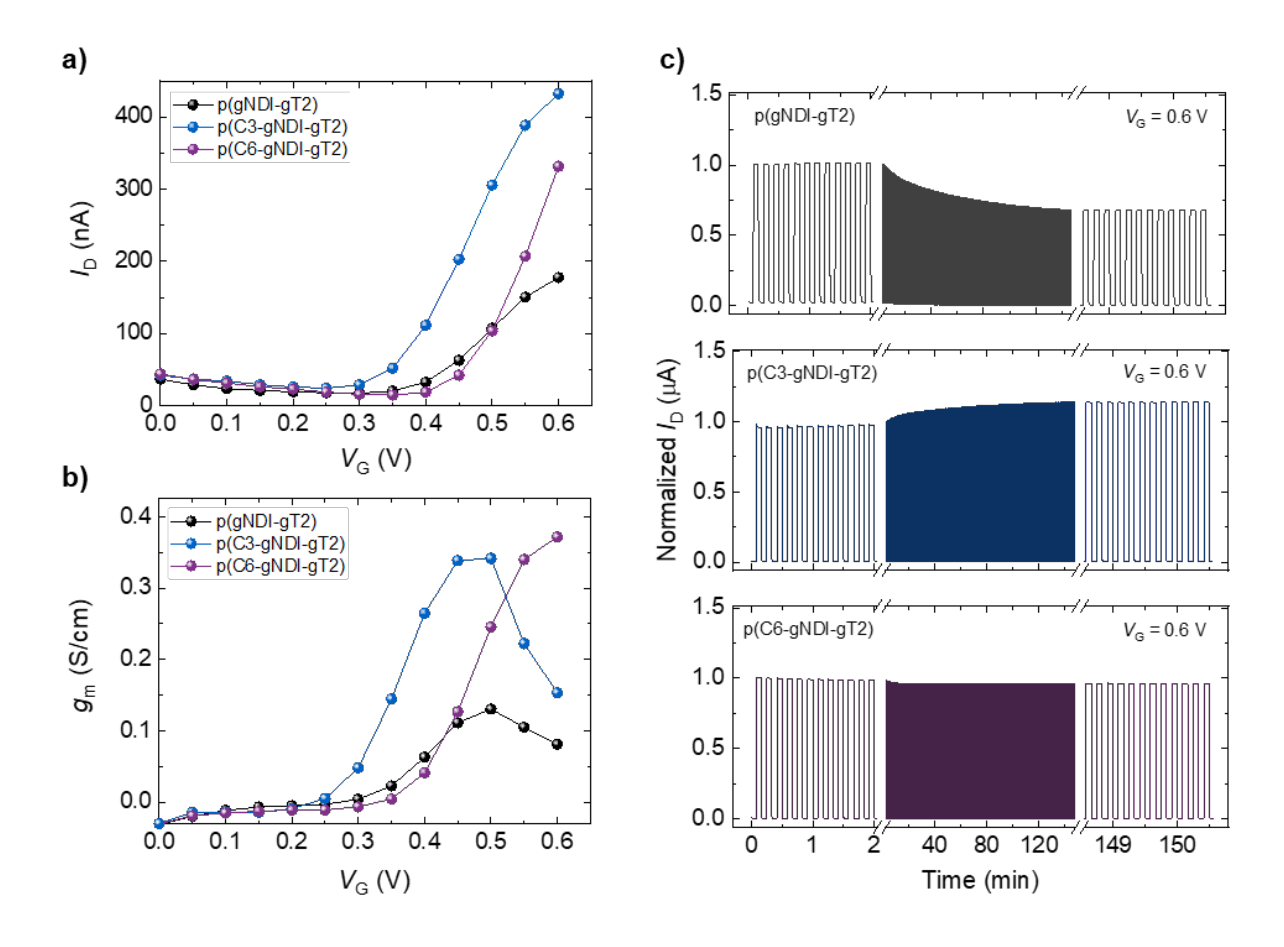


Figure 3. Performance of the OECTs with device dimension ($W = 100 \, \mu m$, $L = 10 \, \mu m$) and a sweep rate of 0.6 V s⁻¹ in 0.1 M NaCl aqueous solution in ambient conditions comprising p(gNDI-gT2) ($d = 55 \, \text{nm}$), p(C3-gNDI-gT2) ($d = 57 \, \text{nm}$) and p(C6-gNDI-gT2) ($d = 46 \, \text{nm}$) in the channel showing (a) n-type transfer curve at $V_D = 0.6 \, \text{V}$ and (b) thickness-normalised transconductance versus gate voltage. (c) Stability pulsing measurements with alternating gate potentials between $V_G = 0 \, \text{V}$ and $V_G = 0.6 \, \text{V}$ for the polymer series with a pulse duration of 5 s for OECT channels biased at $V_D = 0.6 \, \text{V}$ in a 0.1 M NaCl aqueous solution in ambient conditions.

Given the distinct differences in swelling and OECT behavior across the series, it was predicted that the nature of the side chain would also influence the structural changes that the material undergoes in contact with the electrolyte. To investigate this, thin films that had undergone exsitu electrolyte exposure or n-type doping in the aqueous media were analyzed by GIWAXS. It should be noted that while EQCM-D allows for a quantitative determination of the bulk swelling behavior of the polymer, summing swelling of both ordered crystallites and disordered regions, GIWAXS selectively probes the ordered crystallites.

The two-dimensional GIWAXS patterns, line cuts and peak parameters are included in the Supporting Information (Figure S18, Figure S19 and Table S1–S3). All polymers exhibit minimal (>2%) changes in the out-of-plane (010) π -stack and the in plane (001)/(001') backbone d-spacings upon electrolyte exposure and electrochemical reduction, while the inand out-of-plane lamellar d-spacing showed some fluctuations. Analyzing the in-plane backbone scattering, p(gNDI-gT2) shows low lattice parameter fluctuations ($e_{rms} \le 1.0\%$) and fairly steady paracrystalline disorder at ~7% and ~9% for the (001) and (001)' peaks, respectively. This was contrasted with large lamellar lattice parameter fluctuations (~4%) and even larger lamellar paracrystalline disorder (~20%), both of which increased upon electrolyte exposure, resulting in a decrease in the lamellar ξ by ~15%. Electrolyte exposure expanded the in-plane lamellar d-spacing by 1.2 Å, while electrochemical reduction suppressed in-plane lamellar ordering such that only a (100) shoulder in the low q background remained. All combined, p(gNDI-gT2) showed a microstructure with anisotropic disorder, having relatively long-range order along the direction of the polymer backbone that was stable across film conditions, contrasted with much shorter-range order in the direction of lamellar stacking (inplane) that deteriorated upon electrolyte exposure and doping.

As observed for p(gNDI-gT2), p(C3-gNDI-gT2) presented a picture of anisotropic disorder, with a larger decrease in the ξ along the lamellar stacking direction (-42%) than the backbone

direction (-18%) upon electrochemical doping. Though diminished in relative intensity following electrolyte exposure, the in-plane lamellar scattering intensity recovered with electrochemical reduction, showing a lamellar d-spacing expansion of only 0.5 Å.

The d-spacing and relative in-plane lamellar scattering intensity in p(C6-gNDI-gT2) were insensitive to electrolyte exposure and electrochemical reduction. Type I crystallite backbone (001) scattering was absent, while type II ξ extracted from the (001') peak was lower than both p(gNDI-gT2) and p(C3-gNDI-gT2). Across conditions, the lamellar structure of p(C6-gNDI-gT2) showed less non-cumulative disorder (e_{rms}) compared with p(gNDI-gT2) and p(C3-gNDI-gT2), but still lower ξ . Furthermore, disruption of molecular packing was more uniform in p(C6-gNDI-gT2), with both the lamellar and backbone ξ decreasing by ~18% between as cast and electrochemically reduced, compared with the anisotropic disruption in the rest of the series.

Through GIWAXS analysis, it was therefore shown that the degree of distortion of the lamellar lattice spacings and the coherence within crystallites was influenced by the nature of the side chain, where introduction of an alkyl spacer leads to less pronounced lamellar lattice changes but decreased backbone coherence. Interestingly, the structural benefits that seemed to impart improved electron mobility in OFETs did not result in improved performance in OECTs. While p(C3-gNDI-gT2) showed the highest OFET electron mobility and structural features associated with efficient charge transport (larger lamellar and backbone ξ), its OECT performance was comparable to p(C6-gNDI-gT2). These structural benefits were likely eclipsed by disruption of inter-aggregate transport due to a larger extent of swelling for p(C3-gNDI-gT2) relative to p(C6-gNDI-gT2). Similarly, the C6-alkyl spacer, which imparted the lowest swelling with electrolyte exposure and doping, also exhibited the most stable current response during extended operation in OECTs.

Comparing with previously reported n-type materials, both polymers containing hybrid side chains show enhanced device stability relative to fullerene-based small molecules^[50] and comparable stability to the current top-performer, BBL.^[26] When considering their performance as OECT channel materials, the thickness-normalized g_m of both polymers is more than one order of magnitude lower than those typically recorded for BBL.^[26] This is most likely a result of the significantly lower C^* (59 or 72 F cm⁻³ versus ~930 F cm⁻³ for BBL) and the presence of side chains in these polymers. However, polar side chains play an important role in promoting efficient ion migration and hence achieving fast response times in devices.^[18] When comparing with the previously reported polymer with optimized EG side chain density and identical backbone (P-90),^[19] both p(C3-gNDI-gT2) and p(C6-gNDI-gT2) achieve a higher thickness-normalized g_m by a factor of ~1.6 in devices operated under similar conditions. Therefore, this study validates the need for side chain engineering and tuning of swelling ability for improving the performance of n-type OECTs. We envisage that applying the strategy presented herein to alternative backbone motifs, such as more rigid systems,^[51] could lead to higher electron mobilities and hence improve the μC^* and g_m even further.

3. Conclusions

In this work, we study the effect of functionalization with alkyl spacers on the redox activity, OECT performance and stability of n-type polymers by synthesizing two NDI-T2 derivatives containing either a propyl- or a hexyl-spacer within their side chains. Our findings show that the addition of alkyl spacers limits detrimental swelling of polymers in aqueous media while enabling reversible redox-reactions at low potentials. When tested as active materials in n-type OECTs, both polymers show a higher μC^* and enhanced stability compared to the polymer containing exclusively polar side chains. Ex-situ GIWAXS analysis revealed that the nature of the side chain influences the static disorder and coherence length within the crystallites upon

exposure and biasing of the polymers in aqueous electrolytes. This study demonstrates the importance of side chain engineering for developing redox-active polymers and presents an effective strategy to improve the performance and stability of n-type OECT materials.

4. Experimental Section

Polymer synthesis: The synthesis and characterization of the monomers and polymers are outlined in the Supporting Information.

Electrochemical analysis: Cyclic voltammograms were recorded using a standard three-electrode setup connected to a Metrohm Autolab PGSTAT101 potentiostat. A platinum mesh (active area 25×35 mm) and a Ag/AgCl electrode (3 M NaCl/H₂O) were used as the counter and reference electrodes, respectively. The polymers were deposited by spin-coating from chloroform solutions (5 mg mL⁻¹) at 1500 rpm for 1 min on ITO-coated glass substrates. The measurements were carried out in either an anhydrous 0.1 M acetonitrile solution of tetrabutylammonium hexafluorophosphate (TBAPF₆) or a 0.1 M NaCl aqueous solution as the supporting electrolyte at a scan rate of 100 mV s⁻¹ under a nitrogen blanket. The electrolyte solutions were degassed with nitrogen for 15 min prior to the measurements.

Spectroelectrochemical measurements were carried out using the same three-electrode configuration in a 0.1 M NaCl aqueous solution under nitrogen. In this case, the ITO-coated glass slides with spun cast polymer were immersed in a quartz cuvette containing the electrolyte solution. The electrochemical measurements were performed while simultaneously recording the optical spectra using an OceanOptics USV 2000+ spectrometer, which collected the transmitted light through the cuvette from a tungsten lamp used as a probe light source. [2] Electrochemical impedance spectroscopy was performed using polymer films cast on gold substrates (500 \times 500 μ m) as the working electrode, a Pt mesh as the counter and an Ag/AgCl reference electrode coupled to a potentiostat (Metrohm Autolab). The measurements were

carried out in a 0.1 M NaCl aqueous solution in ambient conditions. The spectra were recorded for frequencies from 0.1 Hz to 100 kHz. The volumetric capacitance for each system was extracted by determining the value of the capacitance at 0.1 Hz and dividing it with the film volume (area × thickness).

Grazing Incidence Wide Angle X-ray Scattering; GIWAXS measurements were carried out at the Advanced Photon Source at Argonne National Laboratory on beam line 8-ID-E at room temperature under vacuum with 10.92 keV ($\lambda = 1.135 \text{ Å}$) synchrotron radiation with a 0.14° incident angle and measured with a Pilatus 1M hybrid pixel array detector during 5 s exposures. The 2D GIWXAXS patterns were collected from films spin coated (600 rpm for 60 seconds) from chloroform (5 mg mL⁻¹) on p+doped Si wafer substrates with resistivity of approximately 1-100 Ohm cm⁻¹. Multiple exposures were averaged to create 2D images. Averaged images with different detector z-position were stitched together to fill the vertical gaps between detector chips. Data analysis was carried out with GIXSGUI Matlab toolbox and custom curve fitting code. Ex situ electrolyte exposure of GIWAXS samples was accomplished by covering the film with a large droplet of 0.1 M NaCl aqueous solution for ~30 minutes, then rinsed, and blown dry. Ex situ electrochemical reduction was carried out in a similar fashion except with -0.66 V potential applied between the film (contacted via a silver paste back contact) and a Ag/AgCl pellet in contact with the electrolyte drop as previously reported.^[29] In order to avoid dedoping and ion expulsion, the electrolyte was removed while a reductive bias was still applied. The samples were then rinsed in DI and blown dry without any electrical connection such that electrons cannot escape and coulombic forces are assumed to maintain the retention of dopant ions.

OECT fabrication and characterization: The OECTs were fabricated using previously reported photolithographic procedures. [13,16] All the channels studied in this work had the same geometry, with a width of 100 μ m and length of 10 μ m. The polymer solutions (4 mg mL⁻¹)

were deposited by spin-coating at 1000 rpm for 45 seconds before sacrificial peel off of Parylene C after drying. All measurements were performed using an external Ag/AgCl pellet electrode as the gate in a 0.1 M NaCl aqueous solution in ambient conditions. The I-V characteristics were recorded using a dual-channel source-meter unit (NI-PXI) with a custom-written control code in LabVIEW.

Supporting Information

Supporting Information is available from the Wiley Online Library or from the author.

Acknowledgements

The research reported in this publication was supported by funding from King Abdullah University of Science and Technology Office of Sponsored Research (OSR) under awards no. OSR-2018-CARF/CCF-3079, OSR-2015- CRG4-2572, OSR-2016-CRG5-3003 and OSR-4106 CPF2019. We acknowledge EC FP7 Project SC2 (610115), EC H2020 (643791), and EPSRC Projects EP/G037515/1, EP/M005143/1, and EP/L016702/ 1. A.G. acknowledges funding from the TomKat Center for Sustainable Energy at Stanford University. B.D.P. and J.R. gratefully acknowledge support from the National Science Foundation grant no. NSF DMR-1751308, and J.R. acknowledges support from the Alfred P. Sloan Foundation. Special thanks to Joseph Strzalka and Qingteng Zhang for beam line assistance. This research used resources of the Advanced Photon Source, a U.S. Department of Energy (DOE) Office of Science User Facility operated for the DOE Office of Science by Argonne National Laboratory under Contract No. DE-AC02-06CH11357.

Conflict of interest

The authors declare no conflict of interest.

References

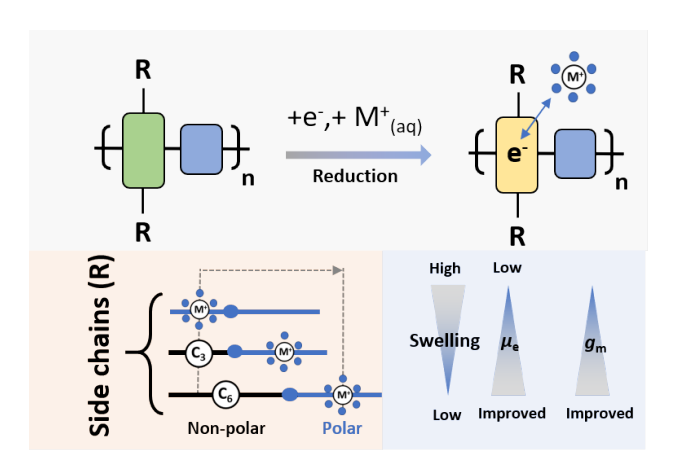
- [1] B. D. Paulsen, K. Tybrandt, E. Stavrinidou, J. Rivnay, *Nat. Mater.* **2020**, *19*, 13.
- [2] D. Moia, A. Giovannitti, A. A. Szumska, I. P. Maria, E. Rezasoltani, M. Sachs, M. Schnurr, P. R. F. Barnes, I. McCulloch, J. Nelson, *Energy Environ. Sci.* **2019**, *12*, 1349.
- [3] A. Malti, J. Edberg, H. Granberg, Z. U. Khan, J. W. Andreasen, X. Liu, D. Zhao, H. Zhang, Y. Yao, J. W. Brill, I. Engquist, M. Fahlman, L. Wågberg, X. Crispin, M. Berggren, *Adv. Sci.* **2016**, *3*, 1500305.
- [4] A. M. Österholm, J. F. Ponder, J. A. Kerszulis, J. R. Reynolds, *ACS Appl. Mater. Interfaces* **2016**, *8*, 13492.
- [5] Y. van de Burgt, E. Lubberman, E. J. Fuller, S. T. Keene, G. C. Faria, S. Agarwal, M. J. Marinella, A. Alec Talin, A. Salleo, *Nat. Mater.* **2017**, *16*, 414.
- [6] A. Melianas, T. J. Quill, G. LeCroy, Y. Tuchman, H. v Loo, S. T. Keene, A. Giovannitti, H. R. Lee, I. P. Maria, I. McCulloch, A. Salleo, *Sci. Adv.* **2020**, *6*, eabb2958.
- [7] J. F. Ponder, A. M. Österholm, J. R. Reynolds, *Chem. Mater.* **2017**, *29*, 4385.
- [8] S. Inal, J. Rivnay, A.-O. Suiu, G. G. Malliaras, I. McCulloch, *Acc. Chem. Res.* **2018**, *51*, 1368.
- [9] E. Zeglio, A. L. Rutz, T. E. Winkler, G. G. Malliaras, A. Herland, *Adv. Mater.* **2019**, *31*, 1806712.
- [10] D. T. Simon, E. O. Gabrielsson, K. Tybrandt, M. Berggren, Chem. Rev. 2016, 116, 13009.
- [11] D. Ohayon, S. Inal, Adv. Mater. 32, 2001439.
- [12] X. Strakosas, M. Bongo, R. M. Owens, J. Appl. Polym. Sci. 2015, 132.
- [13] D. Khodagholy, J. Rivnay, M. Sessolo, M. Gurfinkel, P. Leleux, L. H. Jimison, E. Stavrinidou, T. Herve, S. Sanaur, R. M. Owens, G. G. Malliaras, *Nat. Commun.* **2013**, *4*, 2133.
- [14] S. Inal, G. G. Malliaras, J. Rivnay, Nat. Commun. 2017, 8, 1.
- [15] C. B. Nielsen, A. Giovannitti, D.-T. Sbircea, E. Bandiello, M. R. Niazi, D. A. Hanifi, M. Sessolo, A. Amassian, G. G. Malliaras, J. Rivnay, I. McCulloch, *J. Am. Chem. Soc.* 2016, 138, 10252.

- [16] A. Giovannitti, D.-T. Sbircea, S. Inal, C. B. Nielsen, E. Bandiello, D. A. Hanifi, M. Sessolo, G. G. Malliaras, I. McCulloch, J. Rivnay, *Proc. Natl. Acad. Sci.* 2016, 113, 12017.
- [17] P. Schmode, A. Savva, R. Kahl, D. Ohayon, F. Meichsner, O. Dolynchuk, T. Thurn-Albrecht, S. Inal, M. Thelakkat, *ACS Appl. Mater. Interfaces* **2020**, *12*, 13029.
- [18] A. Giovannitti, C. B. Nielsen, D.-T. Sbircea, S. Inal, M. Donahue, M. R. Niazi, D. A. Hanifi, A. Amassian, G. G. Malliaras, J. Rivnay, I. McCulloch, *Nat. Commun.* 2016, 7, 1.
- [19] A. Giovannitti, I. P. Maria, D. Hanifi, M. J. Donahue, D. Bryant, K. J. Barth, B. E. Makdah, A. Savva, D. Moia, M. Zetek, P. R. F. Barnes, O. G. Reid, S. Inal, G. Rumbles, G. G. Malliaras, J. Nelson, J. Rivnay, I. McCulloch, *Chem. Mater.* 2018, 30, 2945.
- [20] A. Savva, R. Hallani, C. Cendra, J. Surgailis, T. C. Hidalgo, S. Wustoni, R. Sheelamanthula, X. Chen, M. Kirkus, A. Giovannitti, A. Salleo, I. McCulloch, S. Inal, Adv. Funct. Mater. 2020, 30, 1907657.
- [21] L. R. Savagian, A. M. Österholm, J. F. Ponder, K. J. Barth, J. Rivnay, J. R. Reynolds, Adv. Mater. 2018, 30, 1804647.
- [22] M. Moser, T. C. Hidalgo, J. Surgailis, J. Gladisch, S. Ghosh, R. Sheelamanthula, Q. Thiburce, A. Giovannitti, A. Salleo, N. Gasparini, A. Wadsworth, I. Zozoulenko, M. Berggren, E. Stavrinidou, S. Inal, I. McCulloch, *Adv. Mater. n/a*, 2002748.
- [23] H. Yan, Z. Chen, Y. Zheng, C. Newman, J. R. Quinn, F. Dötz, M. Kastler, A. Facchetti, *Nature* **2009**, *457*, 679.
- [24] A. M. Pappa, D. Ohayon, A. Giovannitti, I. P. Maria, A. Savva, I. Uguz, J. Rivnay, I. McCulloch, R. M. Owens, S. Inal, *Sci. Adv.* **2018**, *4*, eaat0911.
- [25] D. Ohayon, G. Nikiforidis, A. Savva, A. Giugni, S. Wustoni, T. Palanisamy, X. Chen, I. P. Maria, E. Di Fabrizio, P. M. F. J. Costa, I. McCulloch, S. Inal, *Nat. Mater.* 2020, 19, 456.
- [26] H. Sun, M. Vagin, S. Wang, X. Crispin, R. Forchheimer, M. Berggren, S. Fabiano, *Adv. Mater.* **2018**, *30*, 1704916.
- [27] D. Trefz, A. Ruff, R. Tkachov, M. Wieland, M. Goll, A. Kiriy, S. Ludwigs, *J. Phys. Chem. C* **2015**, *119*, 22760.
- [28] L. Q. Flagg, R. Giridharagopal, J. Guo, D. S. Ginger, *Chem. Mater.* **2018**, *30*, 5380.
- [29] C. Cendra, A. Giovannitti, A. Savva, V. Venkatraman, I. McCulloch, A. Salleo, S. Inal, J. Rivnay, Adv. Funct. Mater. 2019, 29, 1807034.

- [30] R. Giridharagopal, L. Q. Flagg, J. S. Harrison, M. E. Ziffer, J. Onorato, C. K. Luscombe, D. S. Ginger, *Nat. Mater.* 2017, *16*, 737.
- [31] L. Q. Flagg, C. G. Bischak, J. W. Onorato, R. B. Rashid, C. K. Luscombe, D. S. Ginger, J. Am. Chem. Soc. 2019, 141, 4345.
- [32] A. Savva, C. Cendra, A. Giugni, B. Torre, J. Surgailis, D. Ohayon, A. Giovannitti, I. McCulloch, E. Di Fabrizio, A. Salleo, J. Rivnay, S. Inal, *Chem. Mater.* **2019**, *31*, 927.
- [33] H. K. H. Lee, Z. Li, I. Constantinou, F. So, S. W. Tsang, S. K. So, *Adv. Energy Mater.* **2014**, *4*, 1400768.
- [34] Y. Wang, E. Zeglio, H. Liao, J. Xu, F. Liu, Z. Li, I. P. Maria, D. Mawad, A. Herland, I. McCulloch, W. Yue, *Chem. Mater.* 2019, 31, 9797.
- [35] R. Kim, B. Kang, D. H. Sin, H. H. Choi, S.-K. Kwon, Y.-H. Kim, K. Cho, *Chem. Commun.* **2015**, *51*, 1524.
- [36] Y. Shin, H. Komber, D. Caiola, M. Cassinelli, H. Sun, D. Stegerer, M. Schreiter, K. Horatz, F. Lissel, X. Jiao, C. R. McNeill, S. Cimò, C. Bertarelli, S. Fabiano, M. Caironi, M. Sommer, *Macromolecules* 2020, 53, 5158.
- [37] D. Kiefer, A. Giovannitti, H. Sun, T. Biskup, A. Hofmann, M. Koopmans, C. Cendra, S. Weber, L. J. Anton Koster, E. Olsson, J. Rivnay, S. Fabiano, I. McCulloch, C. Müller, ACS Energy Lett. 2018, 3, 278.
- [38] K. Martin, J. Spickermann, H. J. Räder, K. Müllen, *Rapid Commun. Mass Spectrom.* **1996**, *10*, 1471.
- [39] W. Du, D. Ohayon, C. Combe, L. Mottier, I. P. Maria, R. S. Ashraf, H. Fiumelli, S. Inal, I. McCulloch, *Chem. Mater.* **2018**, *30*, 6164.
- [40] H. Langhals, S. Demmig, H. Huber, *Spectrochim. Acta Part Mol. Spectrosc.* **1988**, *44*, 1189.
- [41] R. Steyrleuthner, M. Schubert, I. Howard, B. Klaumünzer, K. Schilling, Z. Chen, P. Saalfrank, F. Laquai, A. Facchetti, D. Neher, *J. Am. Chem. Soc.* **2012**, *134*, 18303.
- [42] S. A. Jenekhe, L. Lu, M. M. Alam, *Macromolecules* **2001**, *34*, 7315.
- [43] Y. M. Gross, S. Ludwigs, Synth. Met. 2019, 253, 73.
- [44] A. Savva, D. Ohayon, J. Surgailis, A. F. Paterson, T. C. Hidalgo, X. Chen, I. P. Maria, B. D. Paulsen, A. J. Petty, J. Rivnay, I. McCulloch, S. Inal, *Adv. Electron. Mater.* 2019, 5, 1900249.
- [45] J. Rivnay, M. F. Toney, Y. Zheng, I. V. Kauvar, Z. Chen, V. Wagner, A. Facchetti, A. Salleo, *Adv. Mater.* **2010**, *22*, 4359.

- [46] M. Brinkmann, E. Gonthier, S. Bogen, K. Tremel, S. Ludwigs, M. Hufnagel, M. Sommer, *ACS Nano* **2012**, *6*, 10319.
- [47] K. Tremel, F. S. U. Fischer, N. Kayunkid, R. D. Pietro, R. Tkachov, A. Kiriy, D. Neher, S. Ludwigs, M. Brinkmann, *Adv. Energy Mater.* **2014**, *4*, 1301659.
- [48] J. Rivnay, R. Noriega, R. J. Kline, A. Salleo, M. F. Toney, *Phys. Rev. B* 2011, 84, 045203.
- [49] J. Rivnay, M. Ramuz, P. Leleux, A. Hama, M. Huerta, R. M. Owens, *Appl. Phys. Lett.* **2015**, *106*, 043301.
- [50] C. G. Bischak, L. Q. Flagg, K. Yan, C.-Z. Li, D. S. Ginger, ACS Appl. Mater. Interfaces 2019, 11, 28138.
- [51] A. Onwubiko, W. Yue, C. Jellett, M. Xiao, H.-Y. Chen, M. K. Ravva, D. A. Hanifi, A.-C. Knall, B. Purushothaman, M. Nikolka, J.-C. Flores, A. Salleo, J.-L. Bredas, H. Sirringhaus, P. Hayoz, I. McCulloch, *Nat. Commun.* 2018, 9, 1.

Table of contents



A fundamental study on side chain engineering of n-type polymers reveals that substitution of polar side chains with hybrid non-polar/polar ones improves the performance of electrochemical transistors. Our study shows that swelling of the active layer must be controlled to guarantee stable device operation during continuous operation.